Identification of monoclinic θ-phase dispersoids in a 6061 aluminium alloy

Karl Buchanan, Joël Ribis, Jérôme Garnier, Kimberly Colas

Identification of monoclinic θ-phase dispersoids in a 6061 aluminium alloy

Karl Buchanan[a,b], Joël Ribis[a], Jérôme Garnier[a] and Kimberly Colas[b]

[a]DEN-Service de Recherches Métallurgiques Appliquées, CEA, Université Paris-Saclay, F-91191, Gif-sur-Yvette, France

[b]DEN-Service d'Etudes des Matériaux Irradiés, CEA, Université Paris-Saclay, F-91191, Gif-sur-Yvette, France

Intermetallic dispersoids play an important role in controlling the 6xxx alloy series' grain distribution and increasing the alloy's toughness. The dispersoid distribution in a 6061 aluminium alloy (Al–Mg–Si) was analysed by transmission electron microscopy, selected area diffraction and energy-dispersive X-ray spectroscopy. The dispersoids had three unique crystal structures: simple cubic (Pm3), body-centred cubic (Im3) and monoclinic (C2/m). While the SC and BCC dispersoids have been well characterized in the literature, a detailed analysis of monoclinic dispersoids has not been presented. Therefore, the current work discusses the chemical composition, crystal structure and morphology of the monoclinic dispersoids.

1. Introduction

The 6xxx aluminium alloy series (Al–Mg–Si) ranks among the most versatile of the age-hardened aluminium alloys due to the series' high specific strength, formability, weldability and corrosion resistance. As a result, 6xxx series alloys are commonly used within the architectural, marine, automotive, aerospace, recreational and nuclear domains with particular research interest being currently generated by the automotive industry's use of these alloys as body-sheet materials [1]. The 6061-T6 aluminium alloy has been selected for the core vessel of the Jules Horowitz Reactor, which is being constructed by CEA in France. This alloy was selected due to its high neutron transparency, low gamma ray-induced heating, high thermal conductivity, high tensile strength, ductility and fracture toughness before and after irradiation [2]. Despite the alloy's high neutron transparency, neutron irradiation can induce transformation and/or dissolution of the precipitate phases, which significantly affects the alloy's mechanical properties [2]. Recently, Flament et al. [3] demonstrated the potential that irradiation has to modify the 6061 alloy's microstructure by reporting the enhancement of a core/shell compositional organization within α-Al(CrFeMn)Si dispersoids after electron irradiation. In order to understand the evolution of the various precipitate

phases within the 6061-T6 alloy during neutron irradiation, a detailed characterization of the alloy prior to neutron irradiation is first necessary.

Heating of 6xxx alloys to the homogenization temperature (typically between 500 and 600 °C) causes alloying additions of manganese and chromium to combine with aluminium, iron and silicon and form a nanoscale distribution (20–500 nm) of intermetallics commonly known as dispersoids. While the 6xxx series alloys' high tensile strengths in the peak-aged condition are largely attributed to needle-shaped Mg–Si-rich precipitates [4], the dispersoids play a significant role in controlling the grain distribution and increasing toughness [5–10]. The dispersoids pin migrating boundaries during annealing, thus inhibiting recrystallization and restricting grain growth [5,6]. They also cause the strain distribution to become more uniform during plastic deformation, which reduces the tendency for intergranular failure and increases toughness [7–10].

The chemical composition and crystal structure of the dispersoids is influenced by the alloy's chemical composition and the annealing conditions [11–15]. Dispersoids in Mn and Mn/Cr containing alloys generally have simple cubic (SC) or body-centred cubic (BCC) crystal structures (a~1.25–1.27 nm) that are isomorphous to the α-AlMnSi ($Pm\bar{3}$) [16] and α-AlFeSi ($Im\bar{3}$) [17] phases. Mn, Cr and Fe can substitute for Mn and Fe in each of these phases with the level of substitution affecting the crystal structure that the dispersoid obtains. Generally, dispersoids with high Mn:Fe, Cr:Fe and (MnCr):Fe ratios have an SC crystal structure, while those with low ratios have a BCC crystal structure [11–15].

Additional phases have been reported in alloys containing increased Cr contents (>0.3wt.%). Lodgaard and Ryum [18] identified the α′-AlCrSi phase (face-centred cubic, a = 1.09 nm, $F\bar{4}3m$ [18,19]) in co-existence with the SC and BCC α-AlCrSi dispersoid phases. Eidhed, Tezuka and Sato [20] reported solely Al_7Cr dispersoids in an alloy with 0.31wt.%-Cr and the co-existence of Al_7Cr and α-$Al_{12}Mn_3Si_2$ dispersoids in an alloy with 0.29wt.%-Cr and 0.37wt.%-Mn. However, no information was given about the identification and crystal structure of the Al_7Cr dispersoids.

In the present work, Cr-rich dispersoids were characterized in a 6061 alloy where Cr was the main dispersoid-forming element. Specific attention has been paid to a new Al–Cr-rich dispersoid phase, which obtains a monoclinic crystal structure. The monoclinic structure is an approximate of the Al–Cr icosahedral quasicrystal (IQC) structure. This approximate structure allowed significant twinning to occur within these dispersoids. The formation of the Al–Cr-rich dispersoids and the twinning of the monoclinic structure is discussed.

2. Experimental procedure

A direct chill cast 6061 alloy (Table 1) with cross-sectional dimensions of 100 x 360 mm and a length of approximately two metres was produced by Constellium (Voreppe, France). The casting was cut into 100 mm × 100 mm × 120 mm blocks that were then subjected to homogenization (4 h at 530 °C and air cooled), hot forging (10 × ~50% compressive reductions at 450 °C), solution annealing (4 h at 530 °C and water quenching) and isothermal

Table 1. 6061 alloy chemical composition (optical emission spectroscopy, balance Al).

wt.%	Si	Mg	Cr	Fe	Mn	Cu	Zn	Ti
AA6061	0.53	0.92	0.23	0.1	0.08	0.2	<0.01	0.06

ageing (12 h at 180 °C) heat treatments. Analytical transmission electron microscope (TEM) analysis of the alloy was performed at CEA Saclay using a FEI Tecnai G2 operated at 200 keV and equipped with a Bruker XFlash® 5030T EDS system and a Gatan Orius™ SC200 digital camera. The TEM foils were electropolished using a Struers TenuPol electropolisher and Struers A2 electrolyte at approximately 273 K and 30 V. Further thinning was performed using the Gatan Precision Ion Polishing system at accelerating voltages between 1.5 and 3 keV and sputtering angles between 4 and 4.5°.

For each identified dispersoid phase, verification of the crystal structure was initially performed on two separate dispersoids with SAD patterns taken from four widely separated zones. Each zone axis pattern was then compared to reference patterns generated in the CaRine Crystallography software package. Further EDS and SAD analysis was then performed on a minimum of 5–10 additional dispersoids for each phase of similar chemical composition to confirm that additional phases were not present within the dispersoid distribution.

3. Results and discussion

The dispersoids typically obtained ellipsoidal, cuboidal and rectangular morphologies that were less than 200 nm in equivalent diameter. Rod-shaped dispersoids approximately 500–1000 nm in length and 50–100 nm in width were also less commonly observed. The spatial distribution of the dispersoids was relatively even throughout the aluminium matrix. SAD analysis determined that the dispersoids had three unique crystal structures: SC ($Pm\bar{3}$), BCC ($Im\bar{3}$) and monoclinic ($C2/m$). While the SC and BCC α-Al(CrFeMn)Si dispersoid phases have been previously identified in 6xxx alloys [13,18,21,22], monoclinic-type dispersoids have not been widely reported. Thus, the current work will focus on the monoclinic dispersoid phase and the analysis of the Cr-rich α-Al(CrFeMn)Si dispersoids will be published elsewhere [23].

Figure 1a and b shows bright-field images of the cuboidal and rod-shaped morphologies typically obtained by the monoclinic dispersoids. While the cuboidal/ellipsoidal type morphologies were dominant in comparison to the rod-shaped morphology, the cuboidal/ellipsoidal morphologies are possibly a result of the rod-shaped dispersoids being viewed end-on. In general, the size of the cuboidal/ellipsoidal-shaped monoclinic dispersoids and α-Al(CrFeMn)Si was similar. However, the monoclinic rod-shaped dispersoids were typically more slender than the rectangular-shaped α-Al(CrFeMn)Si dispersoids.

SAD patterns taken parallel to the [1 0 0], [1 0 1] and [1 1 0] monoclinic zone axes are shown in Figure 2a–c. The SAD patterns and the tilt angles between each zone agreed with those reported for the monoclinic θ-phase (a = 2.5196, b = 0.7574, c = 1.0949 nm, β = 128.43 [24]) that has been commonly identified in studies on phase equilibria or rapidly solidification of Al-rich binary, ternary and quaternary alloys that contain Cr [24–33]. The monoclinic θ-phase has been described as an approximation of the IQC phase that has been identified in rapidly solidified Al alloys [26]. Analysis of the SAD patterns taken from multiple θ-phase dispersoids in the current work determined the cell parameters differed slightly (a = 2.54, b = 0.767, c = 1.099 nm, β = 128.4) from the previously reported parameters [24]. EDS Analysis of the θ-phase dispersoids after dissolution of the Al-matrix determined the dispersoids were primarily composed of Al and Cr at a ratio between 5:1 and 6:1. This ratio is similar to the reported Al_7Cr, $Al_{13}Cr_2$ or $Al_{45}Cr_7$ compositions for

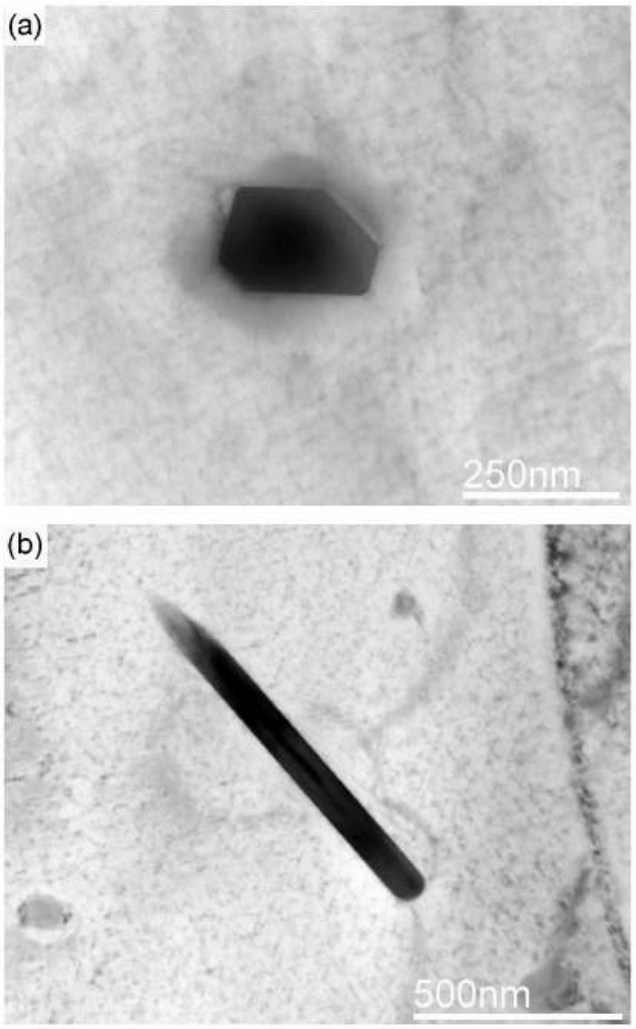

Figure 1. Bright-field TEM micrographs of the (a) cuboidal and (b) rod-shaped θ-phase dispersoids.

θ-phase in binary alloys. Ti and Mn were also detected in low concentrations within these dispersoids. In contrast to the α-Al(CrFeMn)Si dispersoids, silicon and iron were absent from the θ-phase dispersoids.

Figure 3a and b shows bright- and dark-field images of a θ-phase dispersoid that contains multiple planar boundaries that are similar in appearance to twin boundaries. These boundaries were commonly observed within the θ-phase dispersoid distribution. The boundaries extended across the width of the dispersoids and multiple boundaries were always observed within each dispersoid (if the dispersoid contained boundaries). Centring the selected area aperture across the boundaries shown in Figure 3b induced additional reflections within the $[1\,0\,1]_\theta$ SAD pattern (Figure 4a–c). The additional reflections matched those published by Zhang et al. [26] who identified prolific $(\bar{1}\,1\,1)$ and $(1\,1\,\bar{1})$ twinning of θ-phase precipitates in melt-spun Al–Cr alloys. Annealing of the melt-spun alloy at 450 °C caused a progressive transformation of IQCs to crystalline agglomerates of $Al_{45}Cr_7$ (θ-phase). The transformation was considered to be an ordering process that induced the formation of twofold to fivefold rotational twins around the $[1\,0\,1]_\theta$ direction. Twinning around the $[1\,0\,1]_\theta$ direction is possible due to the angle between $(\bar{1}\,1\,1)$ and $(1\,1\,\bar{1})$ being close to 72° (~70.9° [26]). Zhang demonstrated that pseudo-fivefold point group symmetry similar to the fivefold symmetry exhibited by IQCs could be produced by fivefold twinning of the monoclinic crystal

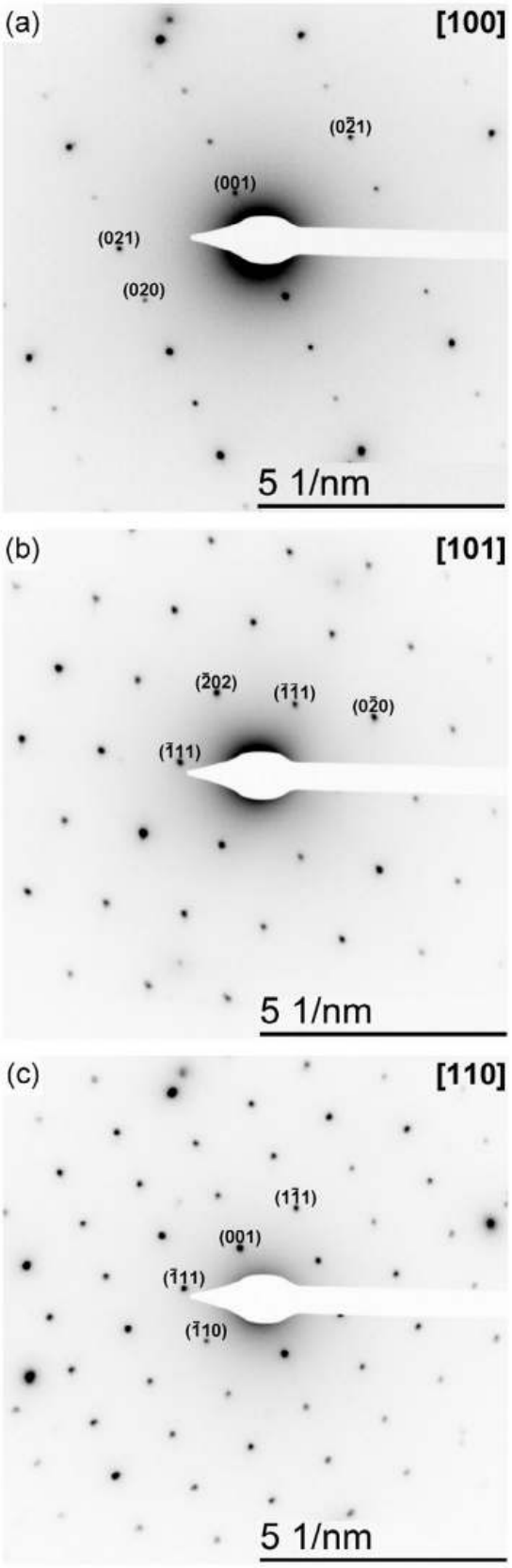

Figure 2. SAD patterns with the beam parallel to the (a) [1 0 0]θ, (b) [1 0 1]θ and (c) [1 1 0]θ directions.

structure around the $[1\,0\,1]_\theta$ direction. Figure 4a and b matches the SAD patterns presented by Zhang [26] for two and threefold rotational twinning around the $[1\,0\,1]_\theta$ direction. Note

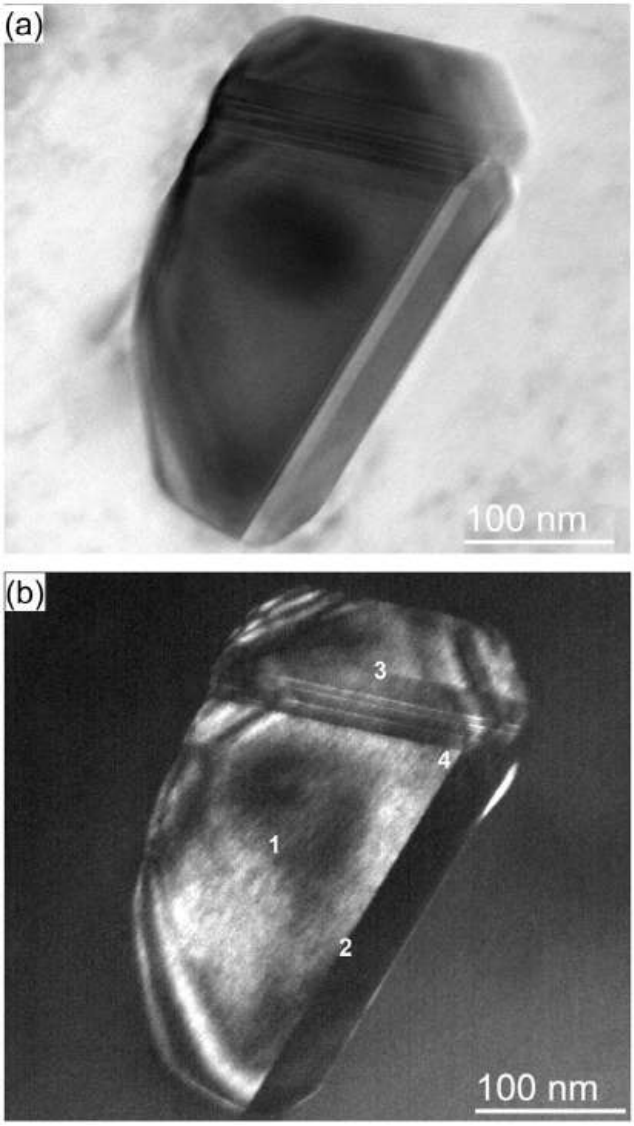

Figure 3. (a) and (b) Bright-field and dark-field (objective aperture centred around $(\bar{2}\,0\,2)\theta$) TEM micrographs of a θ-phase dispersoid containing multiple twin boundaries (beam direction parallel to $[1\,0\,1]\theta$).

that the angle between the intersecting twins in Figure 3b is equal to the angle between the $(\bar{1}\,1\,1)$ and $(1\,1\,\bar{1})$ planes (~71°).

The similar size and morphology of the different dispersoid phases made quantitative measurement of the dispersoid distribution's properties unfeasible for the current publication. However, qualitative observations indicated that the α-Al(CrFeMn)Si dispersoids were more common than the θ-phase dispersoids. The overall spatial distribution of all three dispersoid phases was relatively uniform throughout the aluminium matrix. However, the θ-phase dispersoids were not randomly mixed throughout the overall distribution (i.e. θ-phase dispersoids were surrounded by other θ-phase dispersoids). The non-uniform distribution of θ-phase dispersoids suggests that local compositional gradients within the as-solidified Al-matrix influence the phase that forms during homogenization. Si and Fe were typically absent from the θ-phase composition, both of which are known to segregate during solidification of Al alloys [13,18,33–36]. In contrast, Cr has been shown to be relatively uniformly distributed throughout the Al-matrix in 6xxx alloys [13,18,23]. Hence,

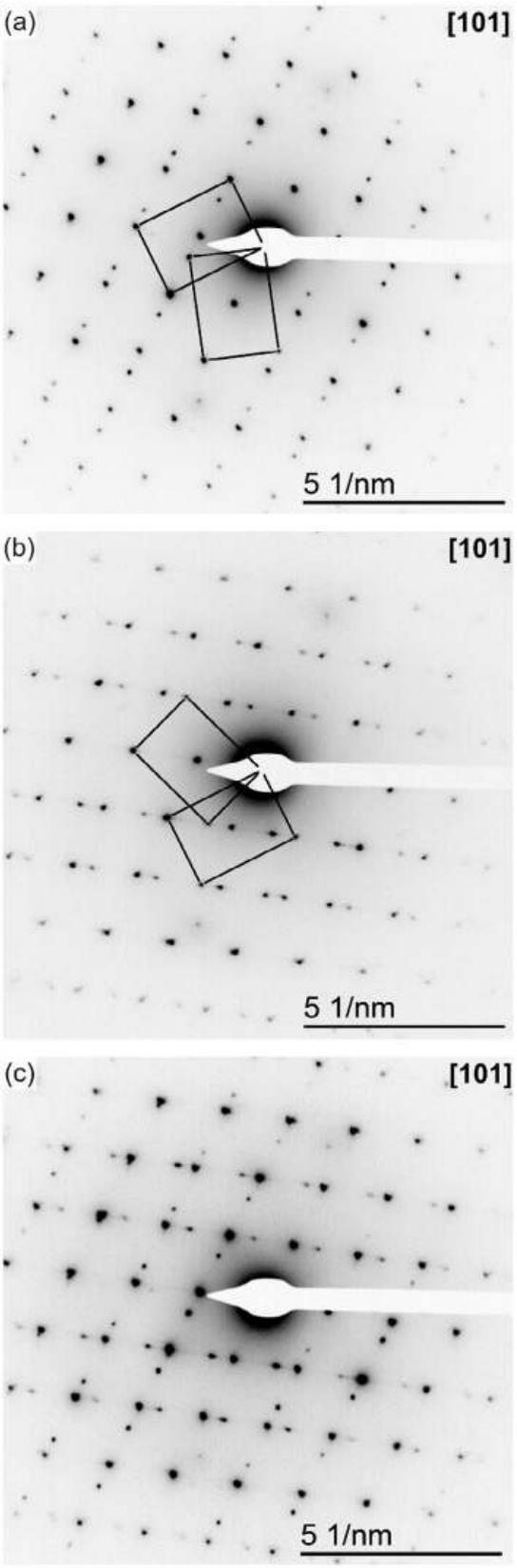

Figure 4. [1 0 1]θ SAD patterns with the SAD aperture centred around points (a) 2, (b) 3, (c) 4 in Figure 6(b). The rectangles in (a) and (b) show the twinning induced ~71° rotation of the [1 0 1] SAD pattern.

the nucleation and growth of the θ-phase dispersoids in place of the α-phase dispersoids could be promoted within regions of the Al-matrix where the concentrations of Si and/

or Fe are particularly low. The solubility of Fe in Al (<0.05wt.% [17]) is relatively low in comparison to Si. Concentrations of 0.2 to 0.4wt.% Si have been reported within the Al dendrite arms after solidification of 6xxx alloys [13,35], whereas the concentration of Fe in the Al-matrix is typically below the resolution of X-ray microprobe analysis [13,18]. Significant Fe segregation in 6xxx alloys has been demonstrated using Scheil calculations [36] and can be indirectly observed by the higher density of α-Al(CrFeMn)Si dispersoids directly adjacent to the primary intermetallics [13,18,36]. Due to the low solubility of Fe (and hence lower availability) in comparison to Si, the nucleation and growth of the θ-phase could be considered to be more dependent on the local concentration of Fe within the Al-matrix. However, Nagahama and Miki [37] determined that the θ-phase precipitation was significantly more prolific in a ternary Al–Cr–Si alloy in comparison to a binary Al–Cr alloy even though the Cr contents were equal for each alloy. Thus, despite the absence of Fe and Si within the θ-phase dispersoids, the segregation of each element likely remains influential during the formation of the θ-phase. Based on the strong segregation of Fe and Si towards the dendrite and grain boundaries, the low solubility of Fe in Al and the relatively uniform distribution of Cr throughout the as-cast aluminium matrix, it is believed that the SC and BCC dispersoids (i.e. the dispersoids containing Fe and Si) will form preferentially within the Al-matrix that is directly adjacent to dendrite or grain boundaries, while the monoclinic θ-phase dispersoids will form preferentially towards the dendrite arm or grain centres (i.e. where the Fe concentration is comparatively negligible).

The nucleation and growth of θ-phase in the current 6061 alloy is believed to occur during homogenization. In general, the Al-matrix of direct chill cast 6xxx alloys is free of dispersoids in the as-cast condition, with nucleation and growth of the dispersoid distribution occurring during homogenization of the cast alloy at temperatures between 500 and 600 °C [13,18,21,22]. Although the formation of θ-phase dispersoids has not been studied in 6xxx alloys, the nucleation and growth of rod-, needle- and plate-shaped θ-phase precipitates is often reported in conventionally cast and rapidly solidified Al–Cr alloys after annealing at temperatures between 400 and 550 °C [32,37–39]. Nagahama and Miki [37] identified the nucleation and growth of needle-shaped θ-phase precipitates on dislocations and sub-grain boundaries after annealing permanent mould cast and cold rolled Al–Cr and Al–Cr–Si alloys at 500 and 550 °C (Al-0.5%Cr and Al-0.5%Cr-0.05%Si, respectively). Furrer and Warilmont [39] directly observed the nucleation of rod-shaped precipitates at quenched-in dislocation loops, while annealing a splat cooled Al-1.2wt.%Cr alloy at 400 °C in the TEM. Thus, the formation of θ-phase from supersaturated solid solution is generally believed to occur on dislocations rather than through the transformation of any transition phase [32,37,38].

The cause of the abundant twinning of the θ-phase dispersoids in the current work is unknown. Despite the common identification of θ-phase precipitates in Al–Cr alloys that are similar in size and shape to the θ-phase dispersoids in the current work, twinning within Al–Cr alloys has not previously been reported. The abundance of θ-phase twinning in the current work suggests it is unlikely that any twinning was present but unnoticed in previous studies of alloys containing θ-phase. The α and α' dispersoid phases identified by Lodgaard and Ryum [18] and θ dispersoid phase identified in the current work are all icosahedral approximate structures and capable of forming twins [26,40,41]. However, twinning of these phases has typically been found in association with IQCs that are present in rapidly solidified Al-transition metal alloys. In the current alloy, twinning appears to be unique to the monoclinic θ dispersoids as the SC and BCC α-phase dispersoids were completely free

of twins. To the best of our knowledge, twinning of the α and α' dispersoid phases in 6xxx alloys has not been published.

Bendersky et al. [40] first identified twinning of icosahedral approximate structures in Al–Mn–Fe–Si alloys. Aggregates of α-$Al_9(Mn,Fe)Si_2$ crystallites that obtained an overall icosahedral symmetry were identified in melt-spun ribbons. Twinning of icosahedral approximate structures has subsequently been observed across an extensive range of rapidly solidified Al-transition metal alloys including Al–Cr [26,33] and Al–Cr-Si [30,41] alloys. Strivastava and Ranganathan [30] proposed three mechanisms through which the twinned aggregates could be formed: direct twinning during growth of the crystalline phase from the liquid; nucleation of the crystalline phase on IQC seeds within the liquid; or through a solid-state transformation that preserves the IQC's orientational order. In general these formation mechanisms result in polycrystalline aggregates rather than the individual rod-shaped precipitates observed in the current work. Additionally, reports of the IQC phase in Al–Cr and Al–Cr–Si alloys have been confined to rapidly solidified alloys [26,30,32,38,41]. Consequently, the twinning within the current work is unlikely related to pre-existing IQCs.

Deformation twins with a planar or lamellar morphology similar to those observed in the current work was observed by Shield and Kramer in Al-Cu-Fe IQCs [42]. High-temperature creep deformation was reportedly enabled by significant twinning of the IQCs. The deformation twins obtained the same fivefold twinning plane that are obtained by as-solidified Al–Mn and Al–Mn–Fe IQCs. Identical planar twinning of IQCs in a rapidly solidified Al–Cu–Fe alloy was also identified by Dai and Urban [43]. While Dai and Urban did not discuss the origin of the twinning, Shield and Kramer suggested it was induced by thermal stresses during cooling. While the θ-phase dispersoids in the current work are believed to form during homogenization of the 6061 alloy at 530 °C, analysis of the θ-phase dispersoids was not performed until after the hot forging (450 °C) and solution annealing (530 °C) stages. In contrast, the analysis of the rod-, needle-, and plate-shaped θ-phase precipitates in binary Al–Cr alloys that formed without twinning was performed directly after annealing [32,37–39]. Based on the current analysis, it is unknown if the plastic deformation during forging induced deformation twinning in the θ-phase or if the plastic deformation is completely accommodated by the Al-matrix. Interestingly, Bendersky et al. [32] determined that the longest axis of the needle and plate-shaped θ-phase precipitates in binary Al–Cr alloys aligned with the $\langle 1\,1\,0 \rangle_{Al}$ direction (i.e. the slip direction for {1 1 1} planes) suggesting a crystallographic orientation relationship (OR) may exist between these two phases. Further investigation into the θ-phase/matrix OR and the possible influence of this OR on deformation twinning of the θ-phase dispersoids during forging of the 6061 alloy is necessary.

4. Conclusion

In summary, the dispersoids in the current 6061 alloy obtained three unique crystal structures, namely simple cubic ($Pm\bar{3}$), body-centred cubic ($Im\bar{3}$) and monoclinic ($C2/m$). The SC and BCC dispersoids were identical to the α-Al(CrFeMn)Si dispersoids previously identified in 6xxx alloys. Monoclinic θ-phase dispersoids were identified in co-existence with the SC and BCC dispersoids. The θ-phase dispersoids where primarily composed of Al and Cr at a ratio between 5:1 and 6:1. In contrast to the α-Al(CrFeMn)Si dispersoids, silicon was notably absent from the θ-phase dispersoids. Twinning of the monoclinic crystal structure

was commonly observed throughout the θ-phase dispersoid distribution. The nucleation and growth conditions for the θ-phase dispersoids during homogenization and effect of this phase on the 6061 alloy's mechanical properties are currently unknown.

Disclosure statement

No potential conflict of interest was reported by the authors.

References

[1] W.S. Miller, L. Zhuang, J. Bottema, A.J. Wittebrood, P. De Smet, A. Haszler and A. Vieregge, Mater. Sci. Eng. A 280 (2000) p.37.
[2] K. Farrell, *Performance of aluminum in research reactors*, in *Comprehensive Nuclear Materials*, R.J.M. Konings, ed., Elsevier Ltd, Amsterdam, 2012, p.143.
[3] C. Flament, J. Ribis, J. Garnier, T. Vandenberghe, J. Henry and A. Deschamps, Philos. Mag 95 (2015) p.906.
[4] R.C. Dorward and C. Bouvier, Mater. Sci. Eng. A 254 (1998) p.33.
[5] R.A. Jeniski Jr., Mater. Sci. Eng. A 237 (1997) p.52.
[6] J.M. Dowling and J.W. Martin, Acta Metall. 24 (1976) p.1147.
[7] J.A. Blind and J.W. Martin, J. Mater. Sci. 18 (1983) p.1224.
[8] J.A. Blind and J.W. Martin, Mater. Sci. Eng. 57 (1983) p.49.
[9] B.J. Dunwoody, D.M. Moore and A.T. Thomas, J. Inst. Met. 101 (1973) p.172.
[10] R.A. Jeniski Jr., B. Thanaboonsombut and T.H. Sanders Jr., Metall. Mater. Trans. A 27 (1996) p.19.
[11] J.E. Yoo, A. Shan, I.G. Moon and S.J. Maeng, J. Mater. Science 34 (1999) p.2679.
[12] A.L. Dons, Scand. J. Metall. 13 (1984) p.137.
[13] L. Lodgaard and N. Ryum, Mater. Sci. Eng.: A 283 (2000) p.144.
[14] P. Donnadieu, G. Lapasset and T.H. Sanders, Philos. Mag. Lett. 70 (1994) p.319.
[15] Z.H. Lai and C.H. Li, Scr. Metall. Mater. 29 (1993) p.895.
[16] M. Cooper and K. Robinson, Acta Crystallogr. 20 (1966) p.614.
[17] M. Cooper, Acta Crystallogr. 23 (1967) p.1106.
[18] L. Lodgaard and N. Ryum, Mater. Sci. Technol. 16 (2000) p.599.
[19] K. Robinson, Acta Crystallogr. 6 (1953) p.854.
[20] W. Eidhed, H. Tezuka and T. Sata, J. Mater. Sci. Tech. 24 (2008) p.21.
[21] K. Strobel, M.A. Easton, L. Sweet, M.J. Couper and J.-F. Nie, Mater. Trans. 52 (2011) p.914.
[22] K. Strobel, E. Sweet, M. Easton, J.-F. Nie and M. Couper, Mater. Sci. Forum 654–654 (2010) p.926.
[23] A. Chbihi, K. Buchanan, J. Ribis and J. Garnier, *Intermetallic dispersoids in aluminium alloy 6061*, 2016, Manuscript in preparation.
[24] M.J. Cooper, Acta Crystallogr. 13 (1960) p.257.
[25] M. Audier, M. Durand-Charre, E. Laclau and H. Klein, J. Alloys Compd. 220 (1995) p.225.
[26] H. Zhang, D.H. Wang and K.H. Kuo, Phys. Rev. B 37 (1988) p.6220.
[27] K.Y. Wen, Y.L. Chen and K.H. Kuo, Metall. Trans. A 23 (1992) p.2437.
[28] B. Grunshko, B. Przepiorzynski and D. Pavlyuchkov, J. Alloys Compd 454 (2008) p.214.
[29] K. Mahdouk and J.-C. Gachon, J. Phase Equilib. 21 (2000) p.185.
[30] A.K. Srivastava and S. Ranganathan, Acta Mater. 44 (1996) p.2935.
[31] J.J. Ramon, D. Shechtman and S.F. Dirnfeld, Scr. Metall. Mater. 24 (1990) p.1087.
[32] L. Bendersky, R.J. Schaefer, F.S. Biancaniello and D. Shechtman, J. Mater. Sci. 21 (1986) p.1889.
[33] V.T. Swamy, S. Ranganathan and K. Chattopadhyay, J. Mater. Res. 4 (1989) p.539.
[34] B. Rinderer, Mater. Sci. Forum 693 (2011) p.264.
[35] M.J. Couper, M. Cooksey and B. Rinderer, Aluminium *cast house technology*, *7th Australian Asian Pacific Conference*, Hobart, 2001, p.287.
[36] S.N. Samaras and G.N. Haidemenopoulos, J. Mater. Process. Technol. (2007) p.63.

[37] K. Nagahama and I. Miki, Trans. Jpn. Inst. Met. (1974) p.185.
[38] K.F. Kobayashi, N. Tachibana and P.H. Shingu, J. Mat. Sci. (1989) p.2437.
[39] P. Furrer and H. Warlimont, Mater. Sci. Eng. (1977) p.127.
[40] L. A. Bendersky, J.W. Cahn and D. Gratias, Philos. Mag. Part B (1989) p.837.
[41] H. Zhang, D.H. Wang and K.H. Kuo, J. Mat. Sci. (1989) p.2981.
[42] J.E. Shield and M.J. Kramer, Philos. Mag. Lett. (1994) p.115.
[43] M.X. Dai and K. Urban, Philos. Mag. Lett. (1993) p.67.